CORNELL UNIVERSITY

Center for Radiophysics and Space Research

ITHACA, N. Y.

CRSR 717

16-39 μ SPECTROSCOPY OF OXYGEN-RICH STARS

by

William J. Forrest
John F. Mc Carthy
James R. Houck

16-39 μ SPECTROSCOPY OF OXYGEN-RICH STARS

by

William J. Forrest
John F. Mc Carthy
James R. Houck

Center for Radiophysics and Space Research
Cornell University

FEBRUARY 1979

Received _____

Abstract

Airborne observations of the 16-39 μ spectra of ten oxygen-rich stars with excess emission in the infrared have been obtained. The stars show excess emission attributed to circumstellar dust grains in the 16-39 μ region in the form of a broad hump peaking near 18 μ and falling smoothly to longer wavelengths. The emission is similar in character to the emission from the Trapezium region of the Orion nebula indicating the grain materials are quite similar in these objects. The existence of a feature in the 20 μ region is consistent with the O-Si-O bending resonance expected for silicate material. The lack of any sharp structure in the spectra indicates the silicate is in an amorphous, disordered form. A simple model of small grains of carbonaceous chondrite silicate material in a diffuse circumstellar envelope is shown to give a good qualitative fit to the observed 8-39 μ circumstellar spectra. Comparison of the observed spectra with the model spectra indicates the grain emissivity falls as $1/\lambda^2$ from 20 μ to 40 μ.

I. Introduction

At wavelengths longward of 8 μ, the spectra of many cool stars show an excess in flux which has been attributed to circumstellar dust emission (Gillett, Low, and Stein 1968; Woolf and Ney 1969). The circumstellar nature of this excess emission has been confirmed by spatially resolving the shells from the star (Zapalla et al 1974, McCarthy et al 1977, Sutton et al 1977) and its identification with dust supported by the lack of any fine structure in high resolution spectra (Gammon et al 1972, Treffers and Cohen 1974). Less certain are the chemical and physical composition of the dust grains, their temperatures and spatial distribution about the star and the wavelength dependence of the opacity of the grains. These characteristics are important to an understanding of the process of grain formation and mass loss from the stars. Further, infrared spectroscopy has shown that the grains around oxygen rich stars are quite similar to an important component of the interstellar dust grains. Thus information on the composition and opacity of the circumstellar dust grains has important applications to the understanding of other galactic infrared sources.

The present study of the 16-39 μ spectra of oxygen rich stars provides new information about the dust grains

in the circumstellar envelopes. If the 10 μ emission feature in circumstellar spectra is due to an Si-O stretching resonance in silicate grains, as suggested by Woolf and Ney (1969), a second O-Si-O bending resonance is expected in the 20 μ region. The shape of the 20 μ resonance depends on the chemical/physical composition of the silicate material. For instance well ordered silicates, as are found on the earth and Moon, all show fine structure in the 20 μ region. The instrumentation and observations are presented in sections II and III and discussed in section IV. A simple shell model of silicate grains is compared with the observed spectra in section V.

II. Instrumentation

The observations were made with helium cooled Ebert-Fastie spectrometers using telescopes aboard NASA aircraft operating between 41,000 and 45,000 ft. altitude. The two channel spectrometer covers the wavelength range 16-39 μ (Forrest, Houck, and Reed 1976). An As:Si detector was used for the 16-23 μ band with a resolution 0.5 μ FWHM. Prior to 1977 the 21-39 μ band used a Ge:Ga photoconductor built by W. J. Moore with a resolution of 1.2 μ FWHM. In February 1977 this was replaced by a more sensitive Ge:Zn detector configured to give a resolution of 1.0 μ FWHM. The 10 channel spectrometer covers the wavelength range 16-30 μ and employs 10 Si:Sb photoconductors with an Intel 8080 microprocessor

based data system which demodulates the signals of 10 detectors simultaneously. This spectrometer and data system are described more fully in a separate paper (McCarthy, Forrest, and Houck 1978). The spectral resolution was 0.2 μ FWHM for all the observations except for the spectrum of VY CMa for which $\Delta\lambda$ = 0.5 μ FWHM. The spectrometers were used in conjunction with the 91 cm telescope of the NASA Gerard P. Kuiper Airborne Observatory (KAO) and the 30 cm telescope of the NASA Lear Jet (VY CMa only). The beam size of approximately 30″ on the KAO and 2.7′-3.2′ on the Lear Jet was large enough to include most of the flux from these compact sources. Standard sky chopping using the oscillating secondary was employed.

III. Observations

The program stars are listed in Table 1 along with their two-micron sky survey number (IRC, Neugebauer and Leighton 1969), their AFGL sky survey number (AFGL, Price and Walker 1976), the spectral and variable type, and an estimate of the fractional amount of the total emission which is in excess of that expected from the star alone ("bolometric excess"). The stars were selected on the basis of their brightness at 20 μ, the presence of the 10 μ "silicate" feature, and spectral evidence in the visible of an oxygen-rich atmosphere

(O/C > 1). With the exception of IRC + 10420 all the stars are luminous, red giant stars probably in an advanced stage of stellar evolution. IRC + 10420 is an unusual and luminous G0 I star with large excess emission from dust (Humphreys et al 1973). OH 26.5 + 0.6 shows evidence of having the thickest dust shell of the stars in this group, with strong absorption at 10 μ and a very cool energy distribution. It is thought to be a Mira variable red giant which is losing mass rapidly (Forrest et al 1978). The stars are arranged here in order of increasing optical depth of the circumstellar material, as judged their fractional bolometric excesses (column (6)). The methods used in deriving this "bolometric excess" is described more fully in section IV.

The observations reported here were obtained between January 1976 and May 1978. The line of sight water vapor column density was monitored aboard the KAO and ranged from 5-20 μ precipitable water vapor. The absence of water vapor features in the derived spectra shows that the absorption features have been adequately removed by the normalization procedure. Shortward of 17 μ, absorption due to terrestrial CO_2 affects the spectrum, and it was necessary to make small differential corrections to account for this. For spectral calibration, the Moon was observed with the same instruments. The Moon was assumed to radiate as a blackbody at a temperature appropriate for the phase of and position of the beam on

the Moon as judged by the 10 μ measurements of Geoffrion et al (1960). For the absolute flux calibration on the KAO, ground-based measurement of the 20 μ flux from non-variable sources were used as follows: May 1976, NGC 7027 ($F_{20\mu}$= 6.2 x 10^{-16}W/cm$^2\mu$, Becklin et al 1973); November 1976, α Ori($F_{20\mu}$= 1.43 x 10^{-15}W/cm$^2\mu$, Morrison and Simon 1973); June 1977, μ Cep ($F_{20\mu}$= 5.8 x 10^{-16}W/cm$^2\mu$, Morrison and Simon 1973); May 1978, α Her ($F_{20\mu}$= 3.7 x 10^{-16}W/cm$^2\mu$, Morrison and Simon 1973). For the Lear Jet and January 1978 KAO observations Mars was used as the flux standard at 20 μ using the model of Wright (1976).

The spectra derived under these assumptions are shown in Figures 1a-1e. The flux levels have been normalized for convenient display. In Table 2 the spectra are listed. Column (1) gives the number of the spectrum which identifies the spectrum in the appropriate figure. Columns 2 and 3 give the name of the star and the date of the observation. Column 4 gives the spectrometer and telescope used and column 5, labeled $F_{20\mu}$, gives the flux level of the horizontal tick mark next to the identification numbers in the figures; it is also the approximate flux level observed at 20 μ. In the cases where the infrared excess is small (Table 1), a considerable fraction of the flux observed is from the stellar photosphere.
To estimate the amount expected from the stellar photosphere alone, photometry from .84 μ to 5 μ was fit with a blackbody

of temperature appropriate to the spectral type and extrapolated to 20 μ. This flux will be denoted $F_{20\mu}$ (star); ratio $F_{20\mu}(\text{star})/F_{20\mu}$ is given in column 6. As an example of the probable contribution of the stellar photosphere, the blackbodies for RX Boo (spectrum #3; Fig. 1b) and μ Cep (spectrum #7, Fig. 1a) are included.

Also included in the figures are ground-based, broad-band measurements of the non-variable sources made by other observers. The agreement is quite good in all cases except for the 33 μ observation of μ Cep (Fig. 1a, spectrum #7) reported by Hagen et al (1975). Their flux level is approximately a factor of two higher than was observed here, though the 25 μ flux levels agree within the errors. A second spectrum of μ Cep taken in January 1978 from 16-30 μ (spectrum #8 in Fig. 1a) agrees quite well in shape and flux with the 16-39 μ spectrum taken in June 1977 in the region overlap. Since μ Cep is not variable in the infrared at 20 μ (Morrison and Simon 1973) and has not displayed any large variations in visual flux from 1974 to 1978 (Mattei, 1978), the discrepancy is probably not due to source variability. It is felt that the measurements reported here are sufficiently reliable to rule out the factor of two excess for μ Cep at 33 μ reported by Hagen et al (1975). This point could be settled by an independent measurement of the 33 μ flux level of μ Cep though this would be

difficult to do from the ground because of the large and time-variable opacity of terrestrial water vapor at these wavelengths.

IV. Discussion

All the stars in this study radiate in excess of what would be expected from the star alone in the 16-40 μ band (Table 2). The probable source of this emission is circumstellar dust heated by stellar radiation. The character of this radiation is a smooth, blackbody-like continuum at long wavelengths with leveling off or downturn shortward of 18 μ, most evident in the cases where the dust emission dominates (e.g. μ Cep Fig. 1a, PZ Cas Fig. 1c, VY CMa and IRC + 10420 Fig. 1e, NML Tau Fig. 1d). As this downturn is more rapid than can result from blackbody emission it indicates a resonance in the emissivity of the dust grains in this region. The spectrum of OH 26.5 + 0.6 (Fig. 1d) shows an absorption feature at around 18 μ which is due to radiation transfer effects in the extremely thick shell surrounding the star as discussed by Forrest et al (1978). When the optical depth is large, a local minimum in flux is observed where the grain emissivity peaks due to the decrease in dust temperature with distance from the star.

The spectrum of RX Boo (Fig. 1b), an M8e semi-regular variable is somewhat different than the other stars in that

the emission is almost flat out to 20 μ and then decreases. Taking into account the stellar contribution at these wavelengths (Fig. 1b, smooth curve), this indicates the dust emission peaks at approximately 19 μ as compared to the peak at approximately 17.5 μ seen in the other stars. This could be due to a different composition of dust grains around this star. Interestingly, the 10 μ spectrum of this star (obtained by Gillett and Forrest 1972, not shown here) is somewhat atypical of M-type stars in that the excess peaks at longward of 9.7 μ and decreases less rapidly beyond the peak. R Leo (Forrest et al 1975) shows a similar behavior.

Elitzur (1978) has proposed a mechanism for the excitation of the main line maser emission of OH at 1665 and 1667 MHz which is seen from many cool oxygen-rich red giant stars. In the present study, the cool stars with thinner circumstellar shells, such as RX Boo, X Her, and R Cas, are typical of this class of object. In his model, the ground state inversion results from a non-equilibrium population of upper rotational levels due to pumping by a radiation field which falls more steeply than $I_\lambda \propto 1/\lambda^5$. These upper levels are populated by photons at wavelengths near λ = 35 μ, 53 μ, 79 μ or 119 μ. Of the stars that have been studied, the emergent spectra of the optically thinnest sources with the hottest apparent dust temperatures (i.e. with a small infrared excess given in Table 1) goes as $F_\lambda \propto (1/\lambda)^4$ from 30-40 μ. In those stars with thick shells the observed flux falls off more slowly than this. Thus it is

not obvious that radiation excitation involving 35 μ photons as proposed by Elitzur (1978) will work. Closer to the star or at longer wavelengths the dust spectrum will probably be steeper but this can be offset by a greater contribution from the star whose spectrum is probably a blackbody in the Rayleigh-Jeans limit and therefore goes as $(1/\lambda)^4$.

The emission from the dust alone around the stars μ Cep, PZ Cas, VY CMa and IRC + 10420 from 8-38 μ is shown in Fig. 2. These stars were chosen because of the large contrast between the dust emission and the estimated stellar emission at these wavelengths.

For μ Cep, the stellar spectrum and excess emission from 8-13.5 μ was taken from Russell et al (1975). Those authors discussed the possibility that some of the emission shortward of 8 μ could be from the circumstellar envelope. The stellar spectrum in the 16-40 μ region was assumed to be the continuation of the blackbody fit to the 5.5-8 μ data and is shown as the smooth curve in Fig. 1a. The difference between the observed flux and this blackbody is attributed to circumstellar emission and is plotted in Fig. 2. Integrated over wavelength, the circumstellar emission comprises less than .05 of the total emission from μ Cep (bolometric excess < .05 , Table 1), indicating a relatively thin circumstellar shell. The subtraction process is most uncertain near 8 μ where the stellar continuum can contribute a major fraction of the observed flux.

PZ Cas was observed from 16-39 μ at the suggestion of F. C. Gillett (1976) who had obtained an 8-13 μ spectrum in

November, 1975 showing a very large dust emission feature peaking at 9.7 μ. Using the broad band measurements from the IRC (Neugebauer and Leighton 1969) and AFGL (Price and Walker 1976) in conjunction with the 8-13 μ and 16-39 μ spectra, it was found that the energy distribution could be fit by a 2500° K blackbody shortward of 5 μ plus an infrared excess longward of 8 μ. The blackbody was assumed to represent the stellar continuum and was subtracted to give the infrared excess shown in Fig. 2. Integrated over wavelength, the infrared excess comprised approximately 0.16 of the total flux observed (bolometric excess ≈ 0.16, Table 1), indicating a moderately thick circumstellar shell. Again this process is most uncertain near 8 μ where the stellar continuum can supply a major fraction of the observed flux. Beyond 10 μ the stellar continuum represents less than 10% of the observed flux. There is an additional uncertainty in the ratio of 10 to 20 μ emission because the photometry and spectrometry were done at different times and this source appears to vary in the infrared. (Table 2, Price and Walker (1976)).

For the stars VY CMa and IRC + 10420, optical depth of the circumstellar shell is large enough to modify the stellar spectrum and a different procedure to estimate the infrared excess was necessary. In these cases the total observed emission was integrated over all wavelengths. In the absence of a circumstellar shell, the spectrum of the star was assumed to be a blackbody of temperature appropriate for

the spectral type (6000°K for IRC + 10420, 2500°K for VY CMa) with the same integrated luminosity as the observed luminosity. Any emission above this flux level is certainly circumstellar excess. For VY CMa the infrared excess integrated over wavelength comprises at least 0.5 of the total flux (bolometric excess $\geq$ 0.5, Table 1) while for IRC + 10420 the bolometric excess was at least 0.88. For IRC + 10420, the star can contribute at most 2% of the flux observed at 8 μ and beyond, so no subtraction was necessary and the total observed flux is plotted in Fig. 2. For VY CMa, the star may contribute as much as 12% to the flux observed at 8 μ but this fraction decreases to less than 4% at 10 μ and beyond. Since the contribution of the star to the observed spectrum is uncertain when the optical depth and geometry of the circumstellar shell are uncertain, the total observed flux is plotted in Fig. 2. It is believed to be primarily due to circumstellar emission but there may be some stellar contribution near 8 μ.

From the derived spectra of 8-39 μ circumstellar emission shown in Fig. 2, the similarity of the circumstellar dust is apparent. There is a peak of emission near 18 μ with a smooth continuum falling towards longer wavelengths indicating a resonance in the grain material near 18 μ. At shorter wavelengths there is the familiar and more prominent 9.7 μ emission feature. The existence of these two resonances is in qualitative agreement with the silicate hypothesis which predicts a feature in the 10 μ region due to the Si-O

stretching resonance and a feature in the 20 μ region due to the 0-Si-0 bending resonance.

The smoothness of the spectra indicates the grain material is different than well-ordered lunar and terrestrial silicates which typically show sharp structure, especially in the 20 μ region (cf Knacke and Thomson 1973, Zaikowski et al 1975). The shape of these spectra is quite similar to that observed in the Trapezium region of the Orion nebula (Forrest and Soifer (1976), Forrest, Houck and Reed (1976)), but with a higher apparent temperature. This is consistent with the idea that the cool oxygen-rich red giant stars are the source of an important fraction of the interstellar dust seen in Orion.

V. Shell Model

A. The Model

In order to make a more detailed comparison of the observed circumstellar spectra in Figure 2 and the theoretical emission some simple models have been considered. In the case where the shell optical depth is not large, the theoretical emission is particularly simple because each grain is observed without attenuation and the radiation field which determines the grain temperature falls as $1/R^2$ beyond a few stellar radii. As there are no sharp resonances in the observed spectra it is not possible at this time to unambiguously identify the grain material which is responsible for the emission. However, the existence of the two features near 10 μ and 20 μ is

consistent with silicate emission and this will be used as a working hypothesis for the present models. It will be shown that using measured grain emissivities from a likely silicate material and a realistic density distribution in the circumstellar envelope gives a good fit to the observed optically thin spectra.

Of the laboratory measurements available at present, the silicate materials which appear most similar to the observed 8-40 μ spectra are the carbonaceous chondrite meteorites Vigarano and Murchison measured by Penman (1976) (cf. Forrest et al 1976). This is physically reasonable because this type of meteorite is believed to represent relatively unprocessed material from the primitive solar nebula. Other carbonaceous chondrite materials (Zaikowski and Knacke, 1975) and an artificially produced amorphous silicate material (Day 1974) show a close similarity to the 10 μ feature but the second peak occurs at longer wavelengths than the feature observed here and by Forrest et al (1976). Penman measured the reflectance from polished samples and applied the Kramers-Kronig principle to derive the optical constants from 5 μ to 40 μ. The emissivities of small spherical grains were calculated using Mie theory. For the present comparison, the emissivities of equal parts of the Vigarno and Murchison material has been taken from Penman (1976), the resultant mass opacity, κ_λ, is shown at the top of Figure 3. The peak mass opacity of approximately 2800 cm^2/gm occurs at 10 μ and a second peak with approximately 1650 cm^2/gm opacity occurs near 18.5 μ.

The flux from a grain of mass m_i, mass opacity κ_λ, at a temperature T_i and a distance D away from the Earth will be

$$F_\lambda^{\,i} = \frac{m_i \kappa_\lambda}{D^2} \quad B_\lambda \ (T_i) \tag{1}$$

where B_λ (T) is the Planck blackbody function (W/cm^2 μ ster). If the circumstellar shell is optically thin at infrared wavelengths, each grain will be seen independently and the total flux observed will be:

$$F_\lambda = \frac{\kappa_\lambda}{D^2} \ \Sigma \ m_i \ B_\lambda \ (T_i) \tag{2}$$

Thus the emergent spectrum is determined by the density of grains in the shell versus distance from the star ρ_d (R) and the grain temperature as a function of distance from the star T_d (R). The temperature of a grain will be determined by energy balance, i.e.

$$\dot{E}_{in} = \dot{E}_{out} \tag{3}$$

In the present case $\dot{E}_{out}$ will be dominated by thermal radiation so

$$\dot{E}_{out} = 4\pi m_i \int_0^\infty \kappa_\lambda \ B_\lambda \ (T_i) \ d\lambda \ . \tag{4}$$

If the circumstellar shell is optically thin in the near infrared ($\lambda\lambda 1 - 5$ μ), $\dot{E}_{in}$ will be dominated by the stellar

radiation field, which falls as $1/R^2$ more than a few stellar radii from the photosphere, i.e.

$$\dot{E}_{in} = \dot{E}_o \ (R_o/R)^2 \qquad (5)$$

where $\dot{E}_o$ is the power input at a distance $R = R_o$ from the star.

Equations (3)-(5) thus define the run of temperature versus distance from the star. In order to evaluate equation (4) it is necessary to know the grain opacity κ_λ at all wavelengths. From 5-40 μ, the opacities from Penman (1976) shown in Figure 3 were used. Shortward of 5 μ, it was assumed the optical constants were constant versus wavelength and the particles were small so $\kappa_{\lambda<5\mu} = \kappa_{5\mu}(\frac{5\mu}{\lambda})$. Beyond 40 μ, it was assumed that the imaginary part of the dielectric constant ε_2 fell as $1/\lambda$ so that $\kappa_{\lambda>40\mu} = \kappa_{40\mu} \ (\frac{40\mu}{\lambda})^2$. At the temperatures of most interest in the circumstellar shells between 100 and 1000° K, more than half of the Planck emission falls between 5 and 40 μ so it is believed these approximations are not critical to the results. Numerical integration of equation (4) showed that $\dot{E}_{out} \propto T^{4.4}$ from T = 160 to 1600° K and $\dot{E}_{out} \propto T^{6.1}$ below 160° K.

The density distribution in the circumstellar shell is less certain. The mass loss rate from a star is given by

$$\dot{M} = 4\pi \ R^2 \ \rho \ (R) \quad v\,(R) \qquad (6)$$

where ρ (R) is the total density and v (R) is the out

flow velocity. Since both the gas and the dust mass loss rates have been observed to be fairly constant from stars of this type (cf. Forrest et al 1975, Weymann 1963) and the circumstellar absorption lines (Deutsch 1960, Weymann 1963) and OH emission lines (Wilson and Barret 1972) indicate the outflow velocity is constant with time, it is expected that $\rho \propto 1/R^2$ in the outer parts of the envelope. Since dust grains are not expected to condense where the density is very low and the dust is momentum coupled to the gas (Gilman 1972), one also expects the dust density $\rho_d \propto 1/R^2$ in the outer parts of the envelope. Close to the point where dust grains begin to condense neither the velocity nor the fractional amount of dust is well known. Fortunately, it will be shown that at the wavelengths of interest beyond 8 μ, the shape of the emergent spectrum doesn't depend strongly on the density distribution near the region of condensation. The point at which dust begins to condense will be denoted $R_o \gtrsim r_*$, where r_* is the stellar radius. Theory (Jones and Merrill 1976) and observation (Zappala et al 1974) indicate $R_o/r_* \gtrsim 3$ for the type of stars considered here. For the purposes of this calculation, it has been assumed that all the dust condensation occurs at R_o (cf. Menietti and Fix 1978). Then if radiation pressure on the grains determines the flow velocity, the dust velocity will be of the form

$$v_d(R) \simeq v_d(R_o) + v_\infty \left(1 - \frac{R_o}{R}\right)^{1/2} \qquad (7)$$

where $v_d(R_o)$ is the initial velocity and $v_d(R_o) + v_\infty$ is the final outflow velocity. Two cases have been considered: $v_d(R_o) >> V_\infty$, which leads to a $\rho_d \alpha 1/R^2$ shell structure, and $v_d(R_o) = 0$, for which $\rho_d \alpha \frac{1}{R^2(1-R_o/R)^{1/2}}$ is infinite at R_o but quickly approaches $1/R^2$ beyond $2\ R_o$.

In a preliminary run of the model with $\rho_d \alpha 1/R^2$ and $T_o = 500°$ K, an interesting effect was discovered when the model was run out to outer limits of 10 R_o, 100 R_o, and 1000 R_o. Though 99% of the total flux comes from within 100 R_o, this region contributes only 90% of the flux at 40 μ and approximately half the flux at 80 μ. Even though the temperature is low (∿ 35-76° K) in the outer layers of this shell, the mass is large, and this region dominates the emission at longer wavelengths. Further from the star than approximately 1000 R_o, two effects are important in determining the emergent spectrum beyond 100 μ. First, heating by the interstellar radiation field will set a minimum temperature of the grains. With the grain emissivity used here, a grain radius of 0.1 μ, $Q_{abs} = 1$, and the interstellar radiation field given by Allen (1973), the minimum temperature is approximately 30° K in the galactic plane. Second, when a mass of interstellar matter equal to that in the circumstellar shell has been swept up, the structure of the shell will be significantly different than the $\rho \alpha 1/R^2$ assumed here. For a space density of 1 H atom/cm^3, an outflow velocity of 10 km/s,

and a mass loss rate of $10^{-5} M_\odot$/yr this happens after approximately 3×10^5 years at a distance $R > 10^4 R_o$ from the star. Since we are interested in the emergent spectrum from 5-40 μ, these effects will not be important and it is sufficient to integrate out to 1000 R_o.

With the density in the shell fixed, the only free parameter in the model is T_o, the dust temperature at the distance R_o from the star where dust forms. This temperature has been varied in order to fit the observed ratio of $F_{10\mu}/F_{18\mu}$ for the shells around PZ Cas and μ Cep (Fig. 2). The temperatures are given in Table 3 and the resulting spectra are compared to the observed spectra in Fig. 3. Also given in Table 3 is the temperature a thin isothermal shell would have in order to give the observed ratio $F_{10\mu}/F_{18\mu}$.

B. Discussion

From Fig. 3 it is seen that the models give a good fit to the observed spectra. In particular, the shape and position of the 10 μ and 18 μ emission features are reproduced. This provides further support to the hypothesis (Woolf and Ney, 1969) that silicate grains are responsible for much of the excess emission from oxygen-rich red giant stars. It also indicates that the grains around these stars are probably made of a disordered, amorphous form of silicates similar to that found in the carbonaceous chondrite meteorites.

From Figure 3 it is seen that there is little difference between the emergent spectra for the two density distributions considered here. This shows that the emergent spectrum is not particularly sensitive to the density distribution near $R = R_o$, where it is least well known. Thus it is felt that the discrepancies between the model and observed fluxes shortward of 9 μ and longward of 20 μ are not due to density effects alone.

Short of 9 μ, the models predict more flux than is seen. This could be due to either lower emissivity of the circumstellar grains at these wavelengths or an over-estimate of the stellar continuum which was subtracted to derive the excess emission. For both PZ Cas and μ Cep, the 8 to 10 μ spectrum had the approximate shape of the model spectrum before subtracting the stellar contribution. This indicates that the circumstellar silicates probably have a sharper feature than the silicates measured by Penman (1976). However, some of the observed 6-8 μ continuum could be due to the hot grains in the inner part of the shell. A measurement of the size of the emitting region at different wavelengths could clarify this point.

Longward of 20 μ, the models predict less flux than is observed. This indicates that the emissivity of the circumstellar grains fall less rapidly than the

silicates measured by Penman (1976). The observed spectra would be fit by an emissivity which fell as $1/\lambda^2$ from 20-40 μ rather than the $1/\lambda^{2.6}$ dependence of the Vigarano and Murchison mixture used here.

VI. Conclusions

The study of the 16-39 μ emission from oxygen-rich red giant stars and IRC + 10420 with excess emission at 10 μ has revealed:

(1) The stars show excess emission in the 16-39 μ region in the form of a broad hump peaking near 18 μ and falling smoothly to longer wavelengths.

(2) Except for possibly RX Boo, the emission from these stars is quite similar in character and qualitatively like the emission seen in the Trapezium region of the Orion Nebula (Forrest et al (1976)). This indicates the grain materials are quite similar in these objects.

(3) Lack of further structure in the 20 μ region prevents an unambiguous identification of the circumstellar material. The observed spectra are consistent with emission from small grains of silicate material similar to the carbonaceous chondrite meteorites in a diffuse circumstellar envelope. Comparison of the spectra with a simple model indicates that the grain emissivity falls as $1/\lambda^2$ from 20 to 40 μ and suggests that some of the observed 6-8 μ continuum could be due to emission from hot grains in the inner part of the circumstellar envelope.

(4) The spectra of μ Cep do not show the 33 μ emission feature reported by Hagen et al (1975).

Acknowledgements

We would like to thank the pilots and staff of the NASA Lear Jet and C-141 Kuiper Airborne Observatory and Gerry Stasavage for their assistance in this project. We thank Daniel A. Briotta, Ray W. Russell and E. E. Salpeter for useful discussions and F. C. Gillett for suggesting the observation of PZ Cas and providing its 8-13 μ spectrum. This work was supported by NASA grants NGR 33-010-182 and NGR 33-010-081.

Table 1

(1) Name	(2) IRC	(3) AFGL	(4) Spectrum	(5) Variability	(6) Bolometric Excess*
α Ori	+10100	836	M2 Iab	SRc	s
X Her	+50248		M6e	SRb	s
μ Cep	+60325	2802	M2e Ia	SRc	s
RX Boo	+30257	1706	M7e-M8e	SRb	s
R Cas	+50484	3188	M6e-M8e	M	s
NML Tau	+10050	529	M6e-M10e	M	m
PZ Cas	+60417	3138	M3 Ia^{+}	SRa	m
VY CMa	-30087	1111	M5e Ib pec.	Lc	l
IRC + 10420	+10420	2390	F8-G0 I^{++}		l
OH 26.5 + 0.6		2205			l

The spectral type and variability type are taken from Kukarkin et at (1969) except as noted:

\+ Humphreys 1970
++ Humphreys et al, 1973

*The bolometric excess is the fractional amount of the total luminosity which appears in excess of that expected from the star alone as described in the text.

s = small = 0 to 0.05
m = moderate = 0.05 to 0.5
l = large = 0.5 to 1.0

Table 2

(1) Spectrum, figure	(2) Name	(3) Date	(4) Note*	(5) $F_{20\mu}$ ($W/cm^2\mu$)	(6)+ $\frac{F_{20\mu}\ (star)}{F_{20\mu}}$
1, 1a	α Ori	Nov. 1976	2, KAO	1.45×10^{-15}	0.41
2, 1b	RX Boo	May 1976	2, KAO	3.8×10^{-16}	0.32
3, 1b	RX Boo	June 1977	2, KAO	3.9×10^{-16}	0.31
4, 1b	RX Boo	May 1978	10, KAO	4.0×10^{-16}	0.30
5, 1c	X Her	June 1977	2, KAO	2.15×10^{-16}	0.33
6, 1c	X Her	May 1978	10, KAO	2.1×10^{-16}	0.33
7, 1a	μ Cep	June 1977	2, KAO	5.8×10^{-16}	0.17
8, 1a	μ Cep	Jan. 1978	10, KAO	6.4×10^{-16}	0.16
9, 1c	PZ Cas	Nov. 1976	2, KAO	2.9×10^{-16}	< 0.1
10, 1c	PZ Cas	June 1977	2, KAO	3.7×10^{-16}	< 0.1
11, 1d	R Cas	Jan. 1978	10, KAO	6.8×10^{-16}	0.22
12, 1d	NML Tau	Jan. 1978	10, KAO	1.28×10^{-15}	< 0.1
13, 1d	OH 26.5 + 0.6	June 1977	2, KAO	1.08×10^{-15}	< 0.1
14, 1e	VY CMa	Jan. 1976	2, Lear	6.8×10^{-15}	< 0.1
15, 1e	VY CMa	Nov. 1976	2, Lear	7.7×10^{-15}	< 0.1
16, 1e	VY CMa	Sept. 1977	10, Lear	8.0×10^{-15}	< 0.1
17, 1e	IRC + 10420	May 1976	2, KAO	2.25×10^{-15}	< 0.1
18, 1e	IRC + 10420	May 1978	10, KAO	2.0×10^{-15}	< 0.1

* Notes (Column 4):

2 = 2 detector 16-39 μ spectrometer
10 = 10 detector 16-30μ spectrometer
KAO = NASA C-141 KAO 91 cm telescope
Lear = NASA Lear Jet 30 cm telescope

+An entry < 0.1 in column 6 means the star contributes less than 10% of the observed flux at 20 μ.

Table 3

Star	$F_{10\mu}/F_{18\mu}$ (Observed)	T_o Thin Shell	T_o $\rho_d = \rho_o/R^2$	T_o $\rho_d = \frac{\rho_o}{R^2(1-R_o/R)^{1/2}}$
PZ Cas	2.95	270°K	400°K	340°K
μ Cep	6.9	470°K	1250°K	860°K

References

Allen, C. W. 1973, Astrophysical Quantities (Third Edition) London: Athlow Press.

Becklin, E. E., Neugebauer, G., and Wynn-Williams, C. G. 1973, Ap. Letters, 15, 87.

Day, K. L. 1974, Ap. J. (Letters), 192, L15.

Deutsch, A. J. 1960, Stars and Stellar Systems, Vol. 6, ed. J. L. Greenstein (Chicago: University of Chicago Press) p. 543.

Elitzur, M. 1978, Astro. Ap., 62, 305.

Forrest, W. J., Gillett, F. C., and Stein, W. A. 1975, Ap. J., 195, 423.

Forrest, W. J. and Soifer, B. T. 1976, Ap. J. (Letters), 208, L129.

Forrest, W. J., Houck, J. R., and Reed, R. A. 1976, Ap. J. (Letters), 208, L133.

Forrest, W. J., Gillett, F. G., Houck J. R., McCarthy, J. F., Merrill, K. M., Pipher, J. L., Puetter, R C., Russell, R. W., Soifer, B. T., and Willner, S. P. 1978, Ap. J., 219, 114.

Gammon, R. H., Gaustad, J. E., and Treffers, R. R. 1972, Ap. J., 175, 687.

Geoffrion, A. R., Korner, M., and Sinton, W. M. 1960, Lowell Observatory Bulletin No. 106, Vol. V, No. 1, p. 1.

Gillett, F. C., Low, F. J., and Stein, W. A. 1968, Ap. J. 154, 677.

Gillett, F. C. 1976, (private communication).

Gilman, R. C. 1972, Ap. J., 178, 423.

Hagen, W., Simon, T. and Dyck, H. M. 1975, Ap. J. (Letters) 201, L81.

Humphreys, R. M. 1970, A.J., 75, 602.

Humphreys, R. M., Strecker, D. W., Murdock, T. L,, and Low, F. J. 1973, Ap. J. (Letters), 179, L49.

Jones, T. W. and Merrill, K. M. 1976, Ap. J., 209, 509.

Knacke, R. F. and Thomson, R. K. 1973, Pub. A.S.P. 85, 341.

Kukarkin, B. V., Kholopov, P. N., Efremov, Yu. N., Kukarkina, N. P. Kurochkin, N. E., Medvedeva, G. I., Perova, N. B., Fedorovich, V. P., and Frolov, M. S. 1969, General Catalogue of Variable Stars, Moscow.

Low, F. J., Rieke, G. H., and Armstrong, K. R. 1973, Ap. J. (Letters), 183, L105.

Mattei, J. A. 1978, AAVSO observations, private communication.

McCarthy, D. W., Low, F. J., and Howell, R. 1977, Ap. J. (Letters), 214, L85.

McCarthy, J. F., Forrest, W. J., and Houck J. R., 1978 in preparation.

Menietti, J. D. and Fix, J. D. 1978, Ap. J., 224, 961.

Morrison, D. and Simon T. 1973, Ap. J., 186, 193.

Neugebauer, G. and Leighton, R. B. 1969, Two Micron Sky Survey (NASA, Washington, D. C.).

Penman, J. M. 1976, MNRAS, 175, 149.

Price, S. D. and Walker, R. G. 1976, "The AFGL Four Color Infrared Sky Survey," AFGL-TR-76-0208.

Russell, R. W., Soifer, B. T., and Forrest, W. J. 1975, Ap. J. (Letters), 198, L41.

Sutton, E. C., Storey, J. W., Betz, A. C., and Townes, C. H. 1977, Ap. J. (Letters), 217, L97.

Treffers, R. R. and Cohen, M. 1974, Ap. J., 188, 545.

Weymann, R. 1963, Ann. Rev. Astron. and Ap., 1, 97.

Wilson, W. J. and Barrett, A. H. 1972, Astro. Ap., 17, 385.

Woolf, N. J. and Ney, E. P. 1969, Ap. J. (Letters), 155, L181.

Wright, E. L. 1976, Ap. J., 210, 250.

Zaikowski, A. and Knacke, R. F. 1975, Ap. and Space Sciences, 37, 3.

Zaikowski, A., Knacke, R. F. and Porco, C.C. 1975, Ap. and Space Sciences, 35, 97.

Zappala, R. R., Becklin, E. E., Mathews, K., and Neugebauer, G. 1974, Ap. J., 192, 109.

Figure Captions

Fig. 1a. The observed 16-39 μ spectra of the oxygen rich supergiants α Ori and μ Cep. The flux calibration and other relevant data are given in Table 2. In this and the other figures statistical error bars representing ± 1 sigma of the mean are shown where large enough to plot. The smooth curve is a 4200° K blackbody extrapolated from the 4-8 μ data of Russell et al (1975) and represents an estimate of the probable contribution of the star to the total observed flux from μ Cep (Spectrum #7) as described in the text. The large open symbols are ground-based broad-band observations from the following sources:

squares (□) Morrison and Simon (1973)

diamonds(◇) Hagen, Simon and Dyck (1975)

triangle(△) Low, Rieke and Armstrong (1973)

The lower diamond at 33 μ refers to the μ Cep spectrum below it (Spectrum #7).

Fig. 1b. The observed 16-39μ spectra of the oxygen rich red giant star RX Boo. The flux calibration and other relevant data are given in Table 2. The smooth curve is a 2500° K blackbody extrapolated from shorter wavelengths and represents our estimate of the stellar contribution to the spectrum just above. The open square (□) is the ground based 20 μ measurement of Morrison and Simon (1973).

Fig. 1c. The observed 16-39 μ spectra of PZ Cas (M3 Ia) and X Her (M6e). The flux calibration and other relevant data are given in table 2. The open square (□) is a

broad band 20 μ measurement of X Her by Morrison and Simon (1973).

Fig. 1d. The 16-39 μ spectra of the Mira variables R Cas, NML Tau (= IK Tau) and OH 26.5 + 0.6. The flux calibration and other relevant data are given in Table 2. Some of the OH 26.5 + 0.6 data here has been reported previously by Forrest et al (1978).

Fig. 1e. The 16-39 μ spectra of the super giant stars VY CMa and IRC + 10420. The flux calibration and other relevant data are given in Table 2. Broad band observations by Hagen et al (1975, diamonds) of VY CMa and Humphreys et al (1973, upside down triangles) of IRC + 10420 are included.

Fig. 2. The excess emission from μ Cep, PZ Cas, VY CMa and IRC + 10420 as described in the text.

Fig. 3. Model fits to the excess emission from PZ Cas and μ Cep (solid lines) as described in the text. The crosses are for a density distribution $\rho_d = \rho_o/R^2$ and the diamonds

for a density $\rho_d = \rho_o \frac{1}{R^2(1-R_o/R)^{1/2}}$. The assumed inner temperatures are, from the top 400° K, 340° K, 1250° K, and 860° K as noted in table 3. The squares are the opacity (κ_λ, cm^2/gm) of the meteorite mixture used in calculating the emergent spectra. The peak opacity of 2800 cm^2/gm occurs at 10 μ.

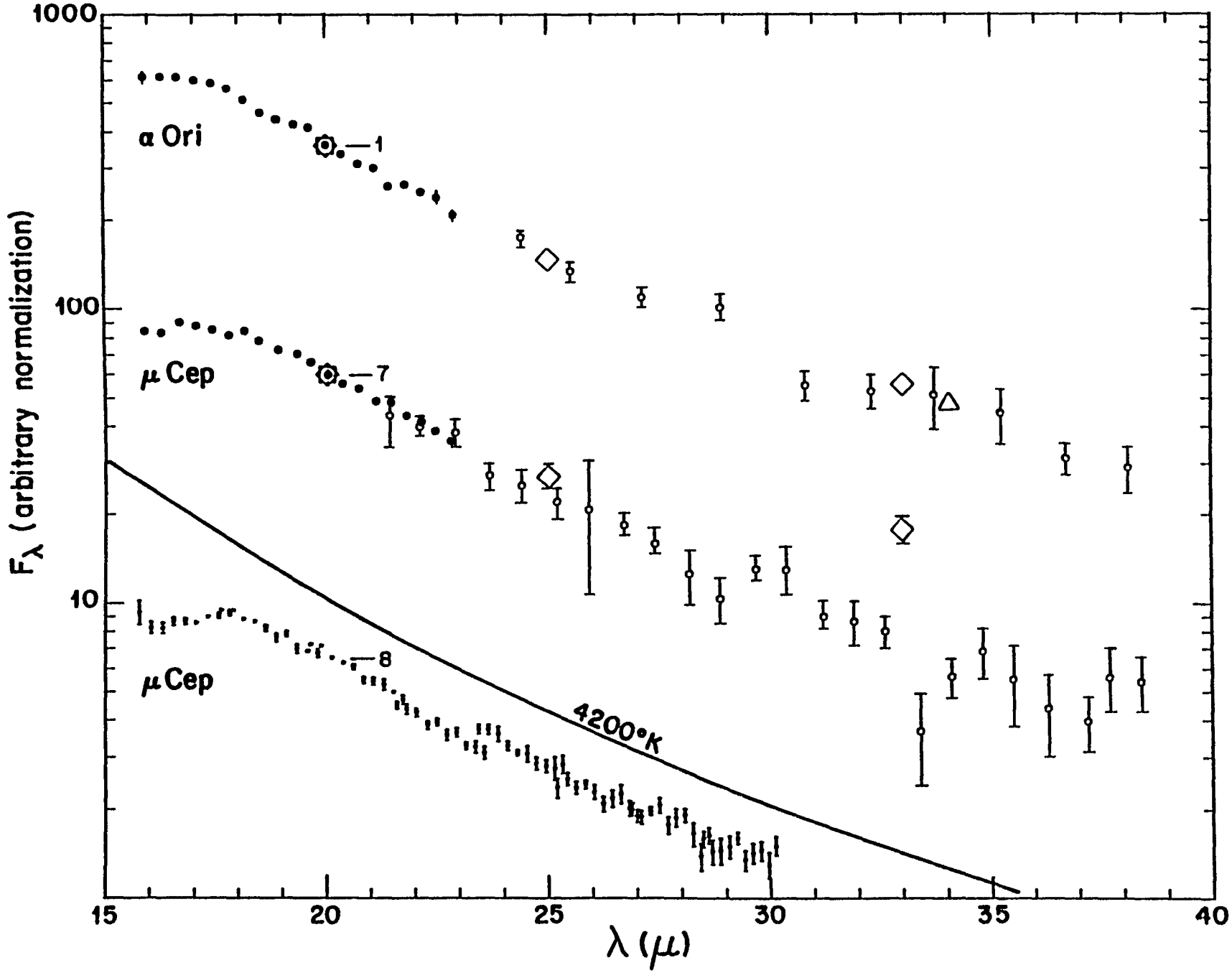
1000
100
10
F_λ (arbitrary normalization)
α Ori
—1
μ Cep
—7
μ Cep
—8
4200°K
15
20
25
30
35
40
λ (μ)

Figure 1a

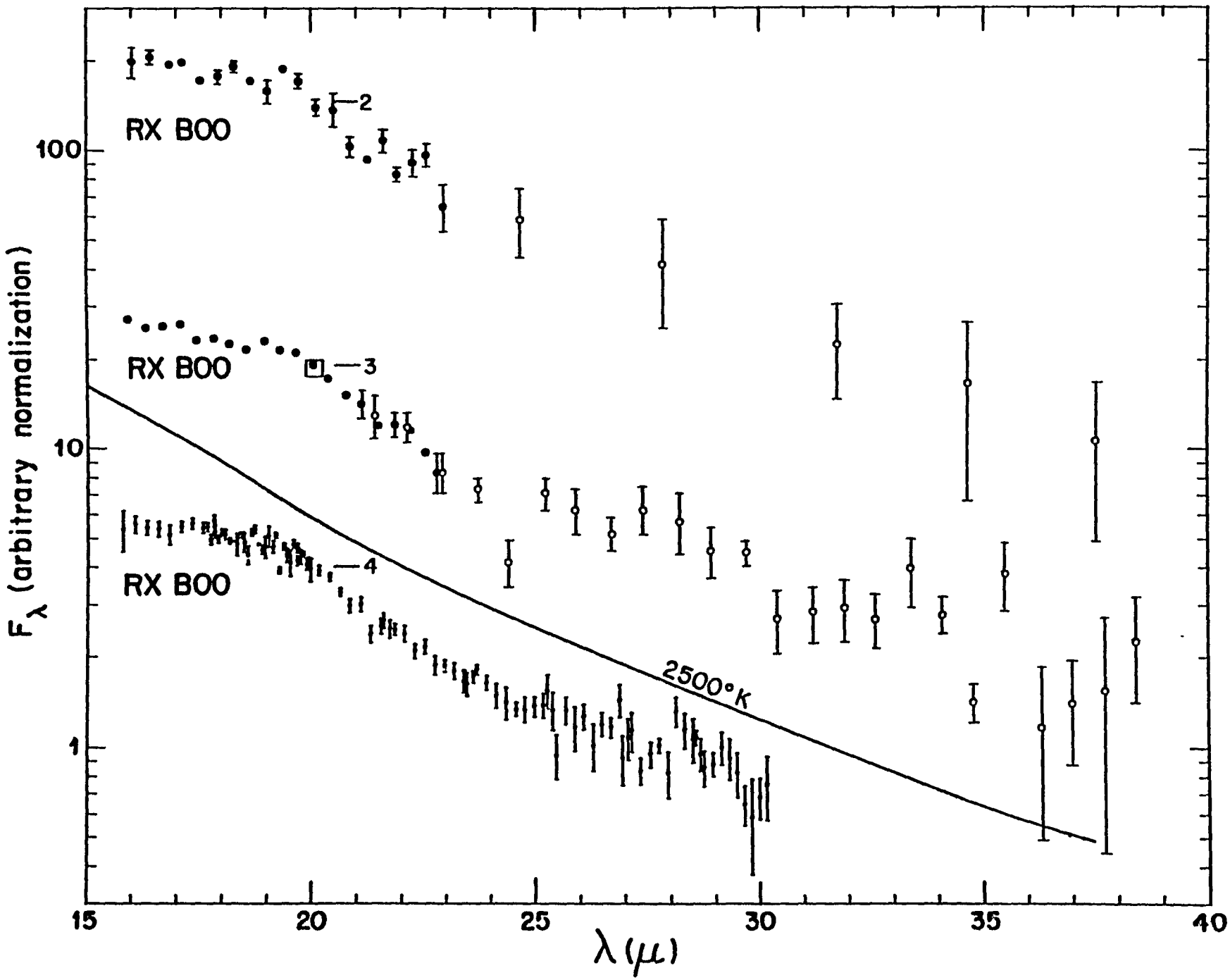
RX BOO
2
RX BOO
3
RX BOO
4
2500°K
100
10
1
15
20
25
30
35
40
F_λ (arbitrary normalization)
$\lambda(\mu)$

Figure 1b

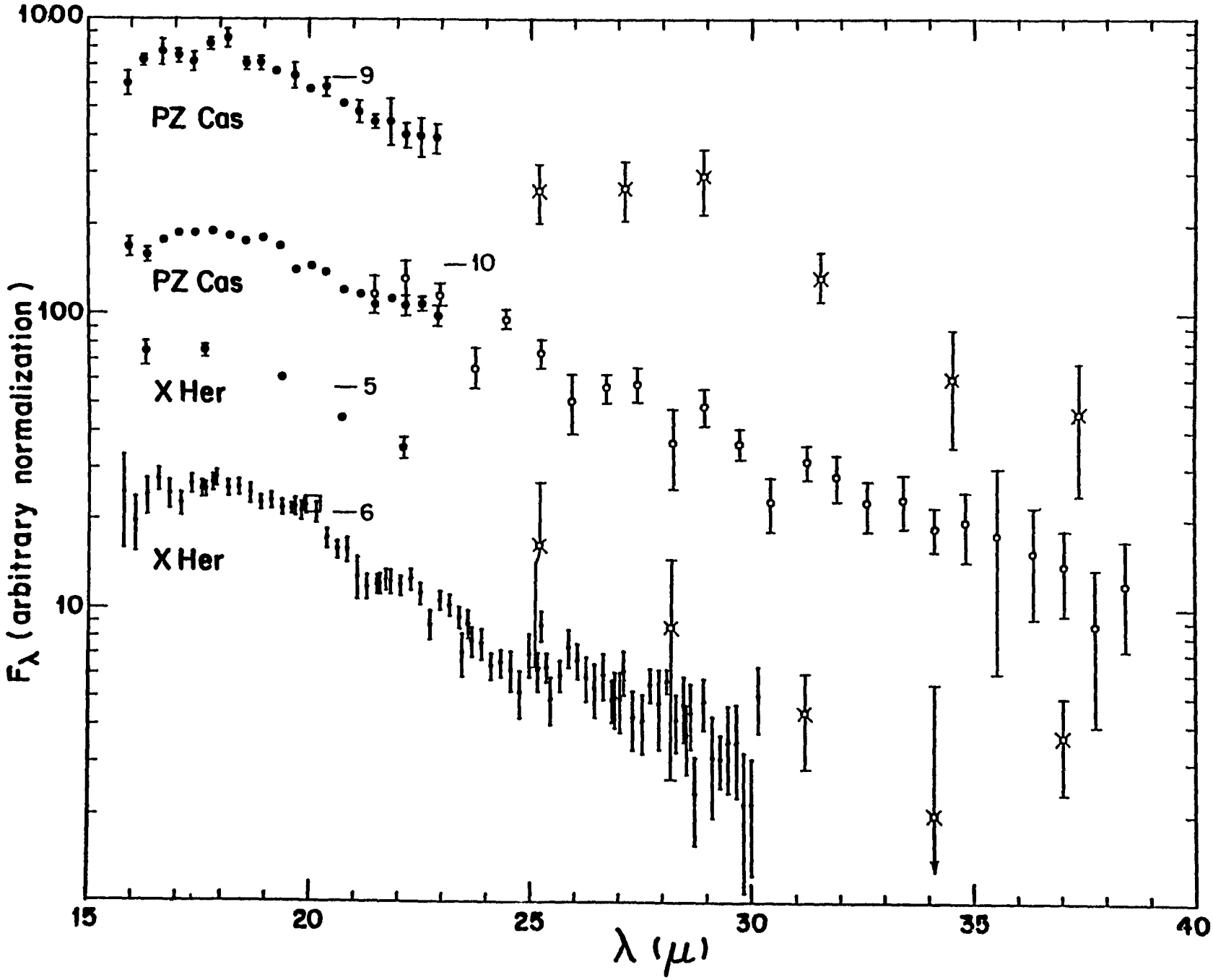
1000
100
10
F_λ (arbitrary normalization)
PZ Cas
—9
PZ Cas
—10
X Her
—5
—6
X Her
15
20
25
30
35
40
λ (μ)

Figure 1c

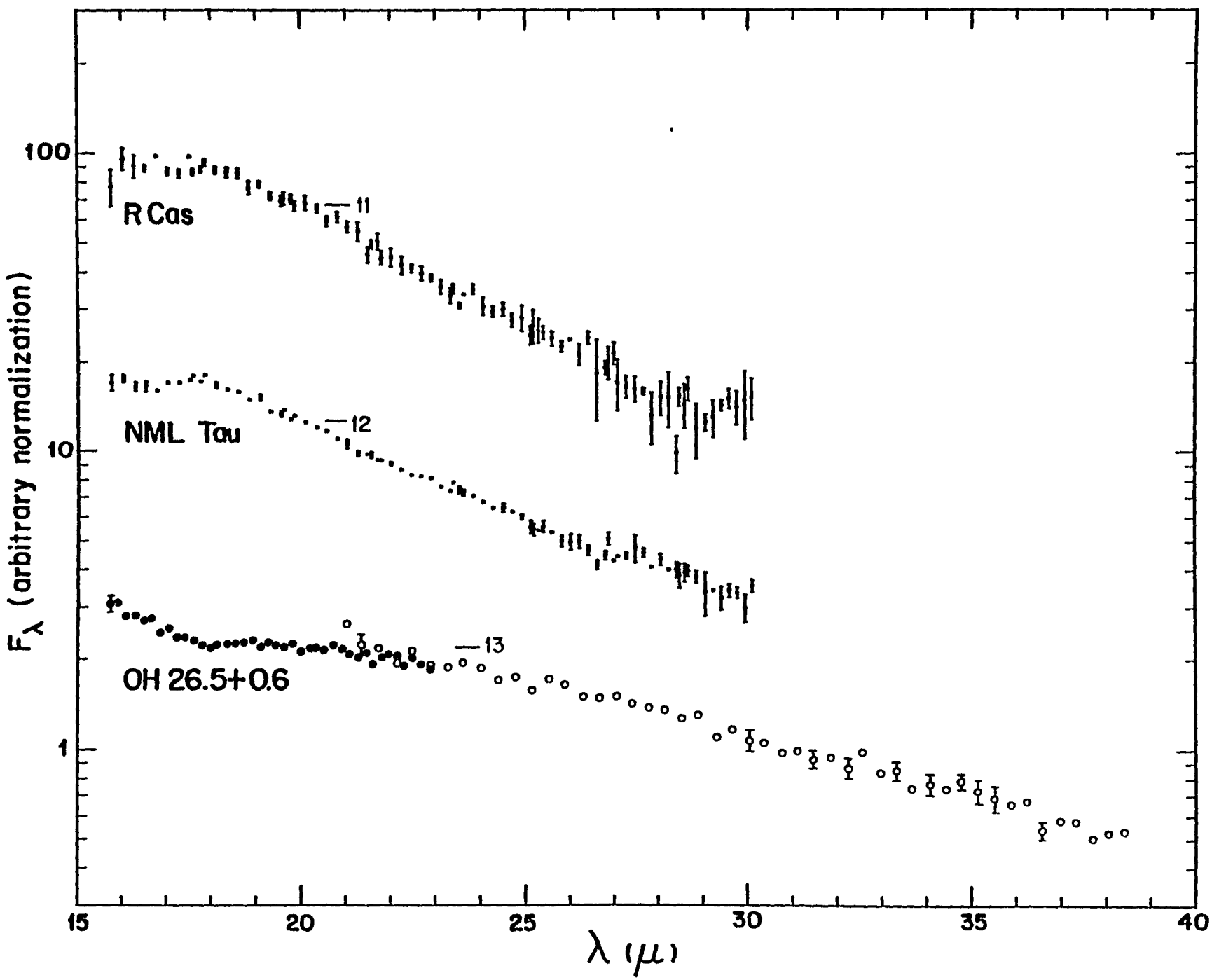
100
10
1
F_λ (arbitrary normalization)
R Cas
—11
NML Tau
—12
OH 26.5+0.6
—13
15
20
25
30
35
40
λ (μ)

Figure 1d

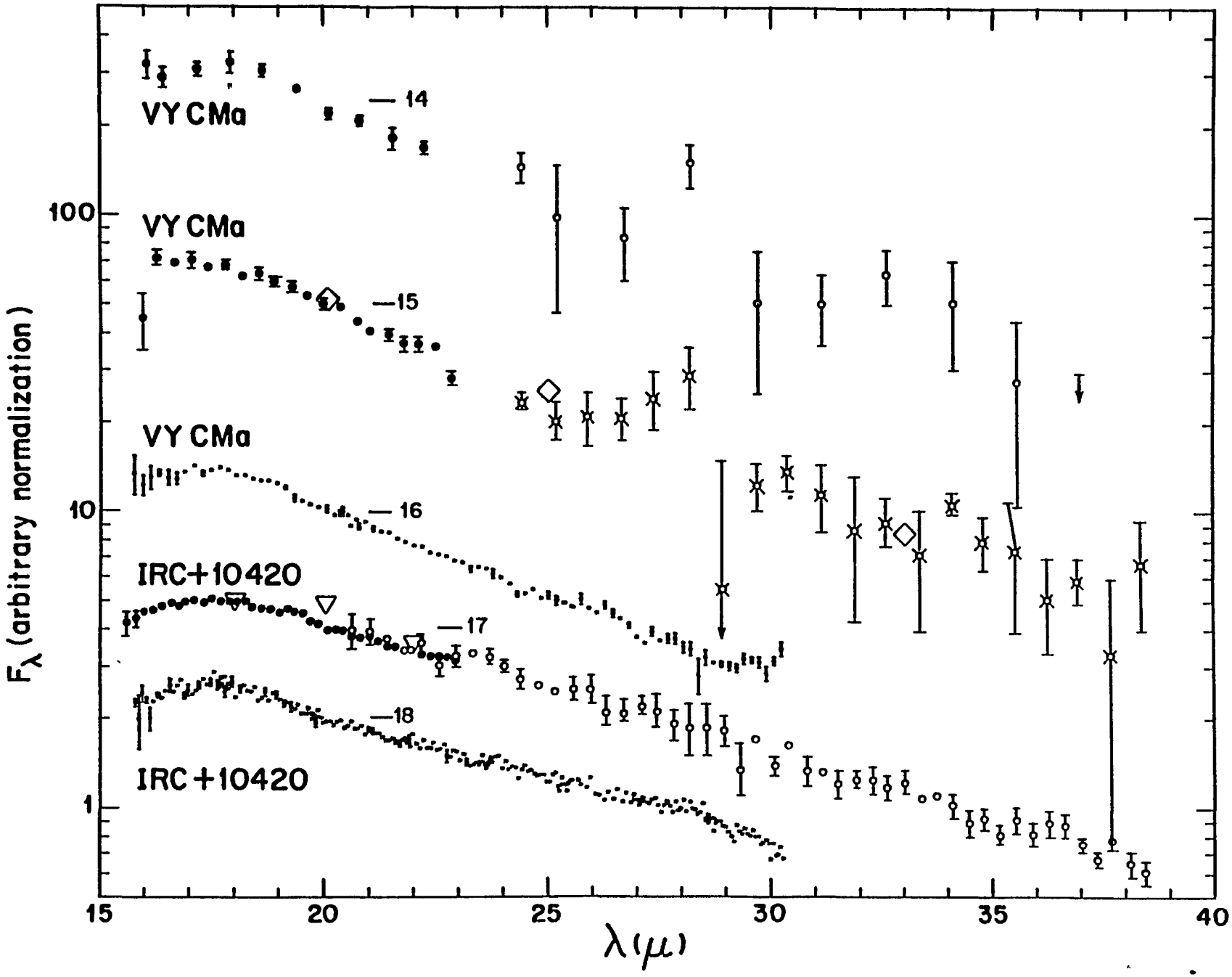
VY CMa
— 14
VY CMa
—15
VY CMa
— 16
IRC+10420
—17
—18
IRC+10420
100
10
1
15
20
25
30
35
40
F_λ (arbitrary normalization)
λ(μ)

Figure 1e

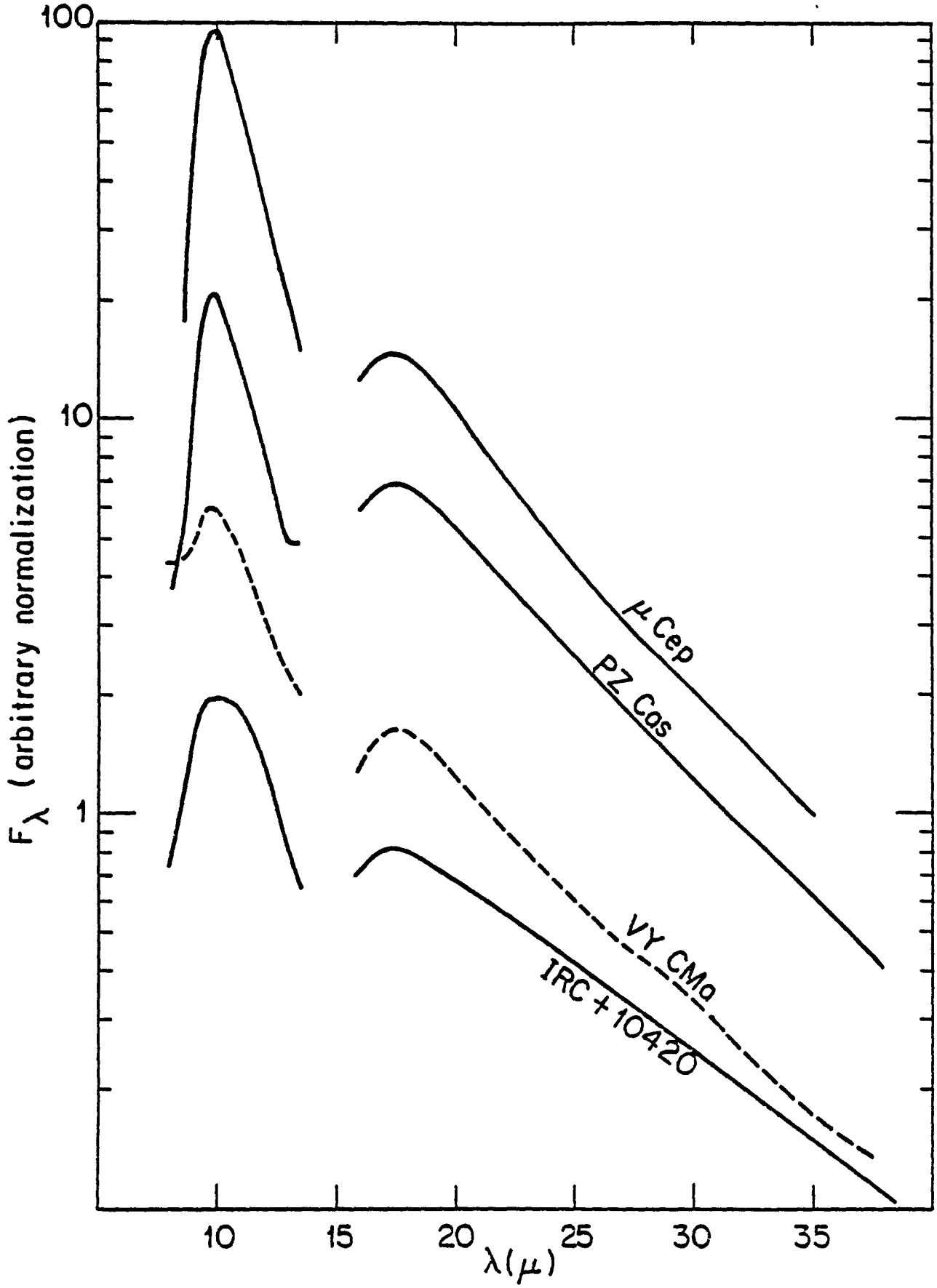
100
10
1
F_λ (arbitrary normalization)
10
15
20
25
30
35
$\lambda(\mu)$
μ Cep
PZ Cas
VY CMa
IRC+10420

Figure 2

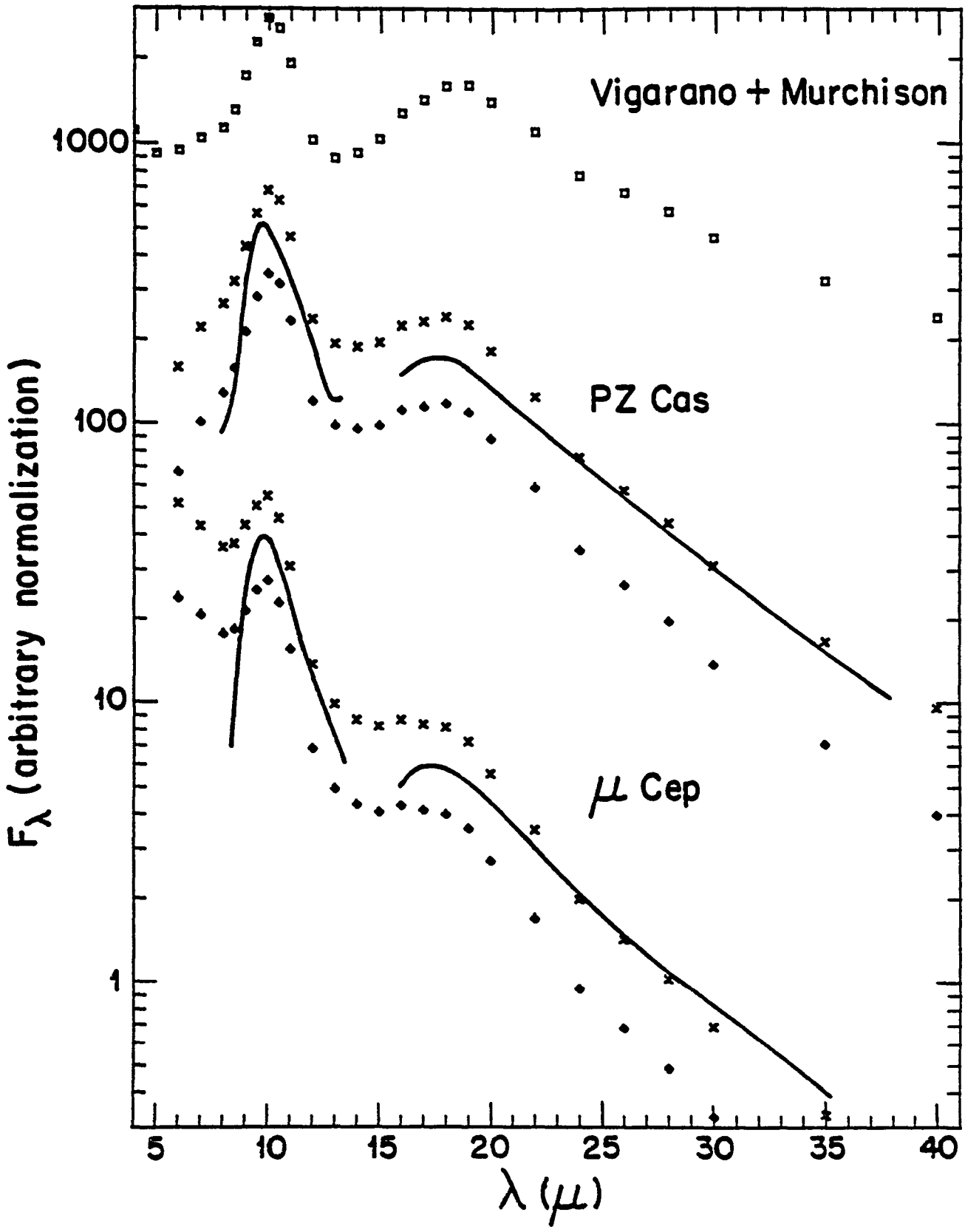
Vigarano + Murchison
PZ Cas
μ Cep
1000
100
10
1
5
10
15
20
25
30
35
40
F_λ (arbitrary normalization)
λ (μ)

Figure 3

End of Document